

Effects of Small Additions of Copper and Copper + Nickel on the Oxidation Behavior of Iron

BRYAN WEBLER, LAN YIN, and SEETHARAMAN SRIDHAR

This study was undertaken to investigate the effect of small amounts of copper and copper + nickel additions on the oxidation rate and oxide/metal interface microstructure of iron. Three iron-based alloys were compared: 0.3 wt pct copper, 0.3 wt pct copper-0.1 wt pct nickel, and 0.3 wt pct copper-0.05 wt pct nickel. Alloy samples were oxidized in air at 1150 °C for 60, 300, and 600 seconds. Pure iron oxidized for 300 seconds was used as a reference material. The parabolic oxidation rate for the iron-copper alloy did not differ from that of pure iron, but the parabolic rate for the nickel-containing alloys decreased by a factor of 2. The microstructure of the iron-copper alloy consisted of a thin, copper-rich layer at the oxide/metal interface. Both nickel-containing alloys had perturbed oxide/metal interfaces consisting of alternating solid/liquid regions. The application of ternary alloy interface stability theories show that the perturbed interfaces arise from unequal diffusivities in the solid γ -iron phase. It is suggested that this perturbed interface microstructure causes the observed decrease in oxidation rate, by limiting the iron supply to the oxide.

DOI: 10.1007/s11663-008-9196-9

© The Minerals, Metals & Materials Society and ASM International 2008

I. INTRODUCTION

LOW-CARBON steel production through scrap melting in an electric arc furnace is an economically^[1] and environmentally^[2] attractive process. However, many issues arise, due to the variation in chemistry that results from use of scrap steel as the input material. A particularly important residual impurity element is copper,^[1] because of its nobility compared to iron and its common presence as a residual element in scrap steel. Since steel is exposed to oxidizing atmospheres (air, CO₂, H₂O) at high temperature for most of its processing prior to hot working, iron selectively oxidizes, enriching the area near the oxide/metal interface in copper.

Considering the iron-copper binary phase diagram shown in Figure 1, copper has limited solubility in solid iron and the new phase that separates is both liquid and copper rich at temperatures greater than 1100 °C. These temperatures occur during secondary cooling, reheating, and hot rolling. According to calculations by Pötschke,^[5] when iron is oxidized in air at temperatures around 1100 °C, the solubility limit of copper in iron is reached in less than one second. Therefore, rapid formation of a copper-rich layer appears to be unavoidable, given the current processing methods for low-carbon steel.

During oxidation, iron dissolves out of the γ -iron phase into the liquid and then it is rapidly transported through the liquid and oxidized at the liquid/oxide

interface. The remaining copper accumulates in the liquid layer and causes it to grow. A small amount of copper also diffuses back into the steel. Because the iron content of the γ iron is high, iron is supplied to the oxide by dissolving more iron into the liquid (*i.e.*, growing the liquid phase), eliminating the need for long-range diffusion to supply the iron. Therefore, processes in the solid and liquid-metal phases should not affect the oxidation rate.

Once the copper-rich liquid forms, it can penetrate into the steel at austenite grain boundaries.^[6] Where penetration has occurred, the boundaries are embrittled by the liquid copper. Intergranular cracking occurs because of this embrittlement, when the steel is subjected to stress during hot working.^[6] This cracking phenomenon is known as surface hot shortness.

Additions of nickel can alleviate hot shortness cracking.^[6] The first beneficial effect of nickel is related to an increase in copper solubility in the γ -iron phase.^[6-8] Figure 2 shows a phase diagram for the iron-copper-nickel system at 1150 °C. Assuming that each component has equal diffusivities, enrichment of the alloy occurs along a straight line defined by the copper/nickel ratio. According to Figure 2, copper/nickel ratios greater than 1 will lead to the appearance of a copper-rich liquid. If the copper/nickel ratio is less than or equal to 1, the entire alloy remains as solid γ iron during oxidation and enrichment. Thus, no hot shortness is expected or observed^[6] in steels with copper/nickel ratios approximately equal to 1 or below. Unfortunately, copper/nickel ratios are greater than 1 for industrially produced low-carbon steels.^[10] The enrichment process for an iron-copper-nickel alloy with a copper/nickel ratio greater than 1 has been described by Akamatsu *et al.*^[11] and is shown schematically in Figure 2.

BRYAN WEBLER and LAN YIN, Graduate Students, and SEETHARAMAN SRIDHAR, Professor, are with the Department of Material Science and Engineering, Carnegie Mellon University, Pittsburgh, PA 15213. Contact e-mail: bwebler@cmu.edu

Manuscript submitted August 8, 2008.

Article published online October 21, 2008.

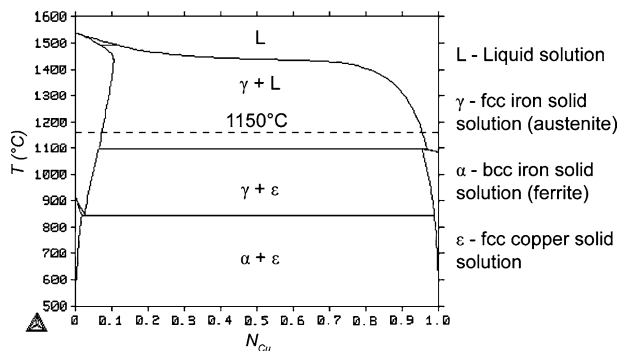


Fig. 1—Binary iron-copper phase diagram generated by Thermo-Calc^[3] (a trademark of Thermo-Calc Software, Stockholm, Sweden) using assessed data.^[4] The names of the various solution phases are also noted.

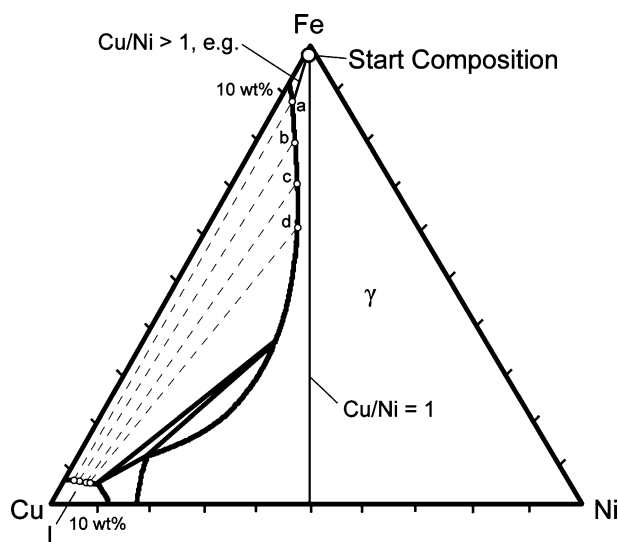


Fig. 2—Ternary phase diagram for the iron-copper-nickel system^[9] at 1150 °C. Points (a) through (d) represent schematically the evolution of interface composition during oxidation, and the dashed lines are tie-lines.

During the initial stages of oxidation, prior to liquid-phase formation and assuming equal diffusivities of iron, copper, and nickel, the composition at the oxide/metal interface will change along a straight line defined by the copper/nickel ratio. In the case of Figure 2, drawn for a copper-nickel ratio of approximately 3, this corresponds to the line that begins at the starting composition and that ends at point “a.” The copper-rich liquid separates at a copper content (point a) higher than the binary iron-copper system, because there is an increase in copper solubility in the iron in the presence of nickel.

Once the γ -iron phase boundary is encountered, the copper-rich liquid phase appears with the compositions in the solid (point a in Figure 2) and liquid at the interface specified by the tie line across the two-phase region. Further oxidation requires redistribution of both copper and nickel from the volume of oxidized γ iron.

Growth of the liquid phase accommodates the copper, as in the binary iron-copper case. However, since the liquid is copper rich, it accommodates only a limited amount of the nickel left behind after the iron is oxidized. Consequently, the remaining nickel accumulates in the solid γ iron near the interface; this drives the interface compositions in the solid from point a to point “d” in Figure 2 (because there are two phases in equilibrium in a three-component system, the interface compositions are not fixed).

The corresponding interface composition in the liquid changes as well, based on the tie lines emanating from points a to “d.” At point d, the inflection point of the phase boundary, nickel can no longer accumulate in the γ -iron phase without violating local equilibrium at the liquid/ γ -iron interface. Therefore, the liquid phase can no longer grow, until the nickel content has been reduced at the interface, due to the solid-state diffusion of the nickel back into the bulk γ -iron phase. The iron supply for continued oxidation now requires either nickel diffusion away from the interface into the bulk solid or the diffusion of iron to the interface from the bulk solid. Consequently, solid-state diffusion in the γ iron is expected to control the oxidation rate.

In the opinion of the present authors, the preceding discussion, first presented by Akamatsu *et al.*,^[11] represents a reasonable qualitative scheme for elucidating the behavior of iron, copper, and nickel during the high-temperature oxidation of iron. It should be noted, however, that the description holds completely true only if the component diffusivities are assumed equal in the γ -iron phase. Experimental results for diffusion coefficients in the iron-copper-nickel system,^[12] however, show that this assumption may not be true. In the iron-rich region, copper diffusivities are higher by as much as a factor of 2. The diffusion coefficients also depend on the alloy composition. Ternary diffusion effects would, therefore, alter the diffusion path in the γ -iron phase between points a and d at one end and the “Start Composition” point at other end, in Figure 2. One major consequence of a change in the diffusion path is that the planar interface between the liquid- and solid-metal phases could become unstable.

In addition to affecting the enrichment behavior, nickel additions promote a beneficial phenomenon known as occlusion^[6,13] This process involves metal enriched in copper and nickel becoming incorporated into the iron-oxide layer. A nickel content of >0.02 wt pct has been found to promote occlusion,^[14] making it a more practical method for reducing hot shortness in industry applications. The occlusion of copper-rich material into the oxide layer has two requirements: the development of a rough oxide/metal interface and the formation of internal oxides that act as lateral bridges between parts of the uneven interface.^[15] Interface roughness is often attributed to the development and stabilization of perturbations in the oxide/metal interface, as analyzed by Wagner.^[16] The formation of a liquid layer at the oxide/metal interface should result in a planar oxide/metal interface,^[17] so nickel has been assumed to delay liquid-phase formation long enough to

allow a rough interface to develop.^[13,15] Nickel also increases the oxygen solubility in the near-interface region, promoting internal oxidation.^[15] Thus, nickel is considered to play a necessary role in both the phenomena that cause occlusion in low-carbon steels. Previous work by the present authors^[18] suggested that nickel alone is not sufficient for achieving significant occlusion during oxidation, for times less than 600 seconds. The current work seeks to isolate the effects of copper and copper + nickel on the oxidation rate and the oxide/metal interface microstructure.

II. EXPERIMENTAL APPROACH

A. Materials

To isolate the effects of copper and nickel, iron-copper and iron-copper-nickel alloys were produced by the Materials Production Center at the Ames National Laboratory (Ames, IA). The alloy chemistries are shown in Table I.

The alloys were arc melted in an inert atmosphere, cold rolled, and cyclically heat treated between 850 °C and 950 °C in an inert atmosphere for 1 hour, to produce a uniform microstructure. A sample Fe was used to establish baselines for the oxidation rate and interface microstructure.

B. Methods

Thermogravimetric (TG) analysis was used to measure the oxidation kinetics. A schematic of the apparatus used is shown in Figure 3(a). Samples were heated in an infrared gold-image furnace. The furnace can achieve high heating and cooling rates by using high energy density halogen lamps to heat samples by radiative heat transfer. The constant-temperature hot zone is 14 cm in length by 1 cm in diameter (temperature range was measured to be ± 1 °C). The hot-zone temperature was measured with a K-type thermocouple inserted into the bottom of the tube. The samples were attached to a balance by a platinum chain, and a sample weight was recorded every second. The results are reported as the mass change per unit surface area.

The high-temperature oxidation was conducted at 1150 °C in air, at a flow rate of 3000 standard cubic centimeters per minute (scm), corresponding to a linear velocity of 12 cm/s. The flow rate was measured with a variable-area flowmeter. The gas velocity was set high enough to minimize the effects of the mass transfer on oxidation rate,^[19] but low enough to prevent the gas from cooling the sample. The results here for pure iron

samples were consistent with those of previous researchers, indicating that neither the mass transfer nor the sample cooling complicated the experimental results. The air used had a water vapor partial pressure of 1.4×10^{-4} atm at 23 °C.

Oxidized sample microstructures were investigated in a scanning electron microscope (SEM). To preserve the interface structure, the samples were mounted in a cold-curing epoxy resin, using the following vacuum-impregnation procedure: (1) samples were placed in a chamber that was subsequently evacuated, (2) the epoxy was added under vacuum, and (3) air was slowly introduced, to force the epoxy into pores and gaps in the oxide. The samples were then sectioned with a low-speed diamond saw and polished to a 1- μ m diamond finish. All samples were coated with 2.5 nm of platinum, to prevent charging in the SEM.

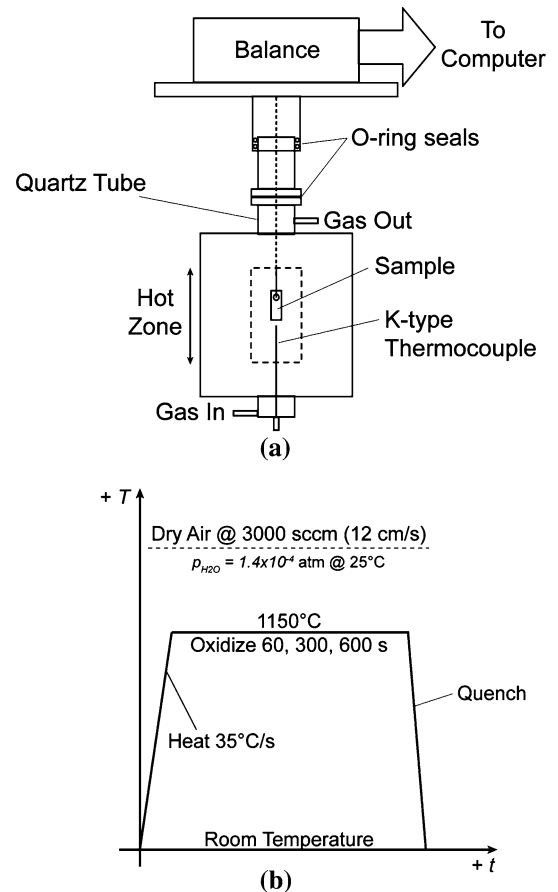


Fig. 3—Schematic of (a) the TG setup and (b) the experimental time-temperature profile used for TG experiments in this study.

Table I. Chemistry (Weight Percent) of Alloys Investigated in This Work

Sample	C	Mn	P	S	Si	Cu	Ni	Cr	Sn	B	Al
Fe	0.001	1×10^{-4}	0.001	1×10^{-4}	5×10^{-4}	4×10^{-4}	1×10^{-4}	2×10^{-4}	1×10^{-4}	1×10^{-4}	1×10^{-4}
Fe-0.3Cu	0.0204	0	0.001	0.002	0.006	0.32	0	0.002	0	0	0.002
Fe-0.3Cu-0.05Ni	0.0185	0	0.001	0.002	0.002	0.32	0.053	0.002	0	0	0.001
Fe-0.3Cu-0.1Ni	0.0206	0	0.001	0.002	0.002	0.3	0.102	0.002	0	0	0.002

The SEM used was a PHILIPS* XL-30 SEM with a

*PHILIPS is a trademark of Philips Electronic Instruments Corp., Mahwah, NJ.

field-emission gun source operating at 25 kV and a solid-state backscattered detector installed. The working distance was 10 mm. All images were taken in backscattered electron (BSE) mode. Energy-dispersive X-ray spectroscopy (EDS) was used to obtain qualitative compositional information.

From the BSE images, the following were quantified.

- Areas of separated copper-rich phase in the metal. These areas appear brighter than the surrounding iron. EDS was used to confirm the presence of copper and nickel.
- Areas of occluded phase. These areas appear brighter than the surrounding oxide.
- Length of the oxide/metal interface.
- Fraction of interface covered by copper-rich liquid.

The open-source software ImageJ (US National Institutes of Health, Bethesda, MD)^[20] was used to measure the quantities listed here. For all measurements, conversion factors were established between the number of pixels and the actual lengths, using the scale bar on the SEM micrograph. The areas of separated or occluded material were isolated, by manually thresholding the images; they were measured using the Wand function (an automatic area trace) of the ImageJ software. These area measurements were then normalized to the length of the field of view (63.2 μm , in all cases). This procedure amounts to considering the separated and occluded area as layers of uniform thickness over a length of 63.2 μm . The results are reported as “amount separated (μm)” or “amount occluded (μm).” The length of the oxide/metal interface was traced by hand and was normalized to the length of a hypothetical flat interface (63.2 μm). The fraction of copper-rich liquid coverage was determined by measuring the length of the contact between the copper-rich liquid and the iron and normalizing it to the measured total interface length. It was often difficult to discern the presence of copper-rich liquid. Measurements of coverage were taken only at locations at which there was reasonable confidence that the copper-rich phase was present; this made the estimate of fraction coverage a conservative one. Measurements were averaged over the oxidation time, for all chemistries. Several measurements were repeated; the error due to reproducibility was found to be negligible.

III. RESULTS

A. Oxidation Behavior

The curves of mass gain per unit area for a 600-second oxidation are shown in Figure 4. A curve for a sample Fe oxidized in 300 seconds is shown as a reference. The oxidation kinetics obeyed a linear rate law:

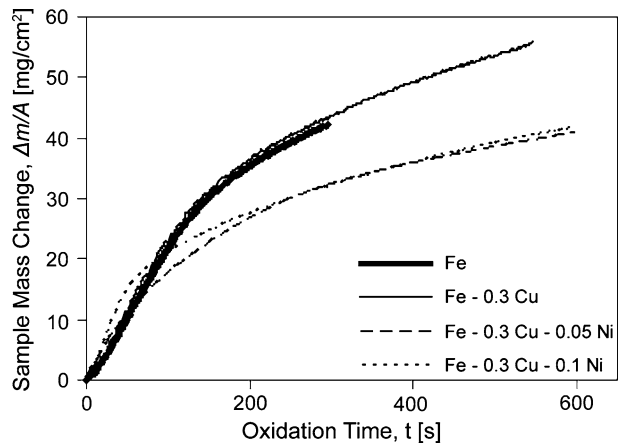


Fig. 4—TG-measured weight change due to oxidation for samples oxidized for 600 s. Pure iron is shown as a reference.

$$\frac{\Delta m}{A} = k_l t \quad [1]$$

where $\Delta m/A$ is the mass gain per unit area, k_l is the linear rate constant, and t is the time, for the first 60 to 70 seconds of oxidation. Linear rate constants were determined by fitting Eq. [1] to the first 60 to 70 seconds of the measured data. The values are shown in Figure 5(a), along with a line representing a calculated rate constant, if the mass transfer of oxygen in the gas phase controls the rate (calculated using equations and data from Abuluwefa *et al.*^[19]).

As oxidation proceeds, the shapes of the curves in Figure 4 change, indicating that a different process controls the oxidation kinetics. The precise extent of the transition region is unknown, but it appears from Figure 4 that this region occurs between 70 and 100 seconds. To eliminate any potential effects of including this transition region, it was assumed to last between 70 and 150 seconds. After oxidation for 150 seconds, the oxidation rate becomes parabolic:

$$\left(\frac{\Delta m}{A}\right)^2 = k_p t \quad [2]$$

All parameters are as defined here except k_p , which denotes the parabolic rate constant. The parabolic regime lasted from 150 seconds until the end of the experiment. Figure 5(b) shows the parabolic rate constants for all chemistries. The constants were determined by fitting a straight line to a plot of $(\Delta m/A)^2$ vs t . The slope of this trend line is related to the parabolic rate constant (Eq. [2]). The squares of the correlation coefficients (r^2 values) for the straight-line fits ranged between 0.98 and 1.00. The line in Figure 5(b) represents the parabolic rate constant of iron calculated by regression of data from the literature.^[21]

From Figure 4, it appears that the presence of copper does not influence the amount of oxide formed compared to pure iron, whereas the presence of nickel decreases the total amount of oxide formed. There is no effect from the amount of nickel, at least for the two

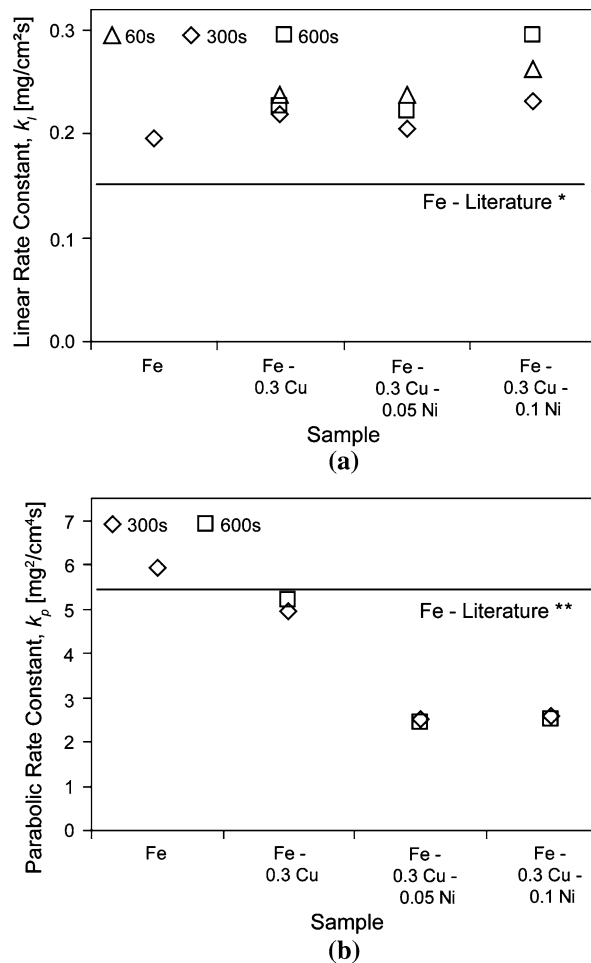


Fig. 5—(a) Linear and (b) parabolic rate constants. *Calculated with equations and data from Abuluwefa *et al.*^[19] **Calculated by regression of data reported by Chen and Yuen.^[21]

nickel-containing samples investigated in this study. From Figure 5, it appears that the effect of nickel on the oxidation rate is primarily a lowering of the parabolic rate constant.

B. Oxide/Metal Interface Microstructure

Example images of the sample microstructure at the oxide/metal interface are shown in Figure 6. In Figure 6, EDS analysis confirmed that the bright areas in the images were copper-rich phases (that would be liquid at 1150 °C); the darker areas were iron rich. Thus, the BSE images clearly distinguish the areas that would be liquid at the experimental temperature of 1150 °C. EDS was also used to determine an estimate for the copper/nickel ratio at the liquid/ γ -iron interface. These values are shown in Table II for both samples and all oxidation times. Measurements were made as close as possible to the interface, but the volume in which the X-rays were generated likely contained some of the copper-rich phase. Thus, the measured copper concentrations are higher (and, therefore, the copper/nickel ratios are higher) than those actually present at the interface.

The images suggest that the interface becomes wavier with time when nickel is present; note the effect of nickel on the interface morphology when comparing Figures 6(b) through (d) and (e) through (j). There is also material found occluded in the oxide. In general, the Fe-0.3 Cu-0.05 Ni and Fe-0.3 Cu-0.1 Ni samples have alternating areas of solid and liquid phases at the interface. Both this interface morphology and an example of occluded material are shown in more detail in Figure 7.

The measurements of the interface length in Figure 8 show that interfaces do, indeed, become wavier, especially after 300 seconds, for the nickel-containing alloys. There is not, however, a substantial change in interface length with increasing oxidation time.

The fraction of interface covered by the copper-rich liquid was quantified from a succession of images of the oxide/metal interface and plotted in Figure 9. As expected from the micrographs in Figure 6, the fractional coverage of copper is significantly higher for the Fe-0.3 Cu sample than for the nickel-containing samples.

C. Amounts of Separated and Occluded Material

The amounts of separated and occluded copper-rich material as a function of time are shown in Figures 10(a) and (b). The plots show that the amount separated is similar for all chemistries after 60 seconds of oxidation, but decreases for the nickel-containing samples as time progresses. The amount of occluded material is small and no distinguishable trends are observed with either time or nickel content. No occluded material is observed in the sample Fe-0.3 Cu.

IV. DISCUSSION

The results presented here show that a small amount of added copper results in a uniform layer of copper-rich phase that does not affect oxidation behavior. Additions of nickel along with copper cause the following: (1) a decrease in the parabolic oxidation rate, (2) an increase in the roughness of the oxide/metal interface, and (3) a decrease in the amount separated and an increase in the amount occluded, compared to a binary iron-copper alloy.

The TG data shown in Figure 4 can be divided into linear and parabolic regimes. During the initial linear stage, the rate-controlling process for oxidation is oxygen diffusion through a gas-phase boundary layer.^[19,22] The development of the equation that describes the diffusion through a boundary layer can be found in the literature (*e.g.*, Levich^[23]). As expected, the linear rates are independent of the alloy chemistry, as shown in Figure 5(a), because the rate-controlling process depends only on the processes in the gas phase. According to Figure 5(b), the presence of copper alone did not affect the parabolic oxidation kinetics, compared to pure iron, while copper + nickel decreased the parabolic rates by a factor of 2.

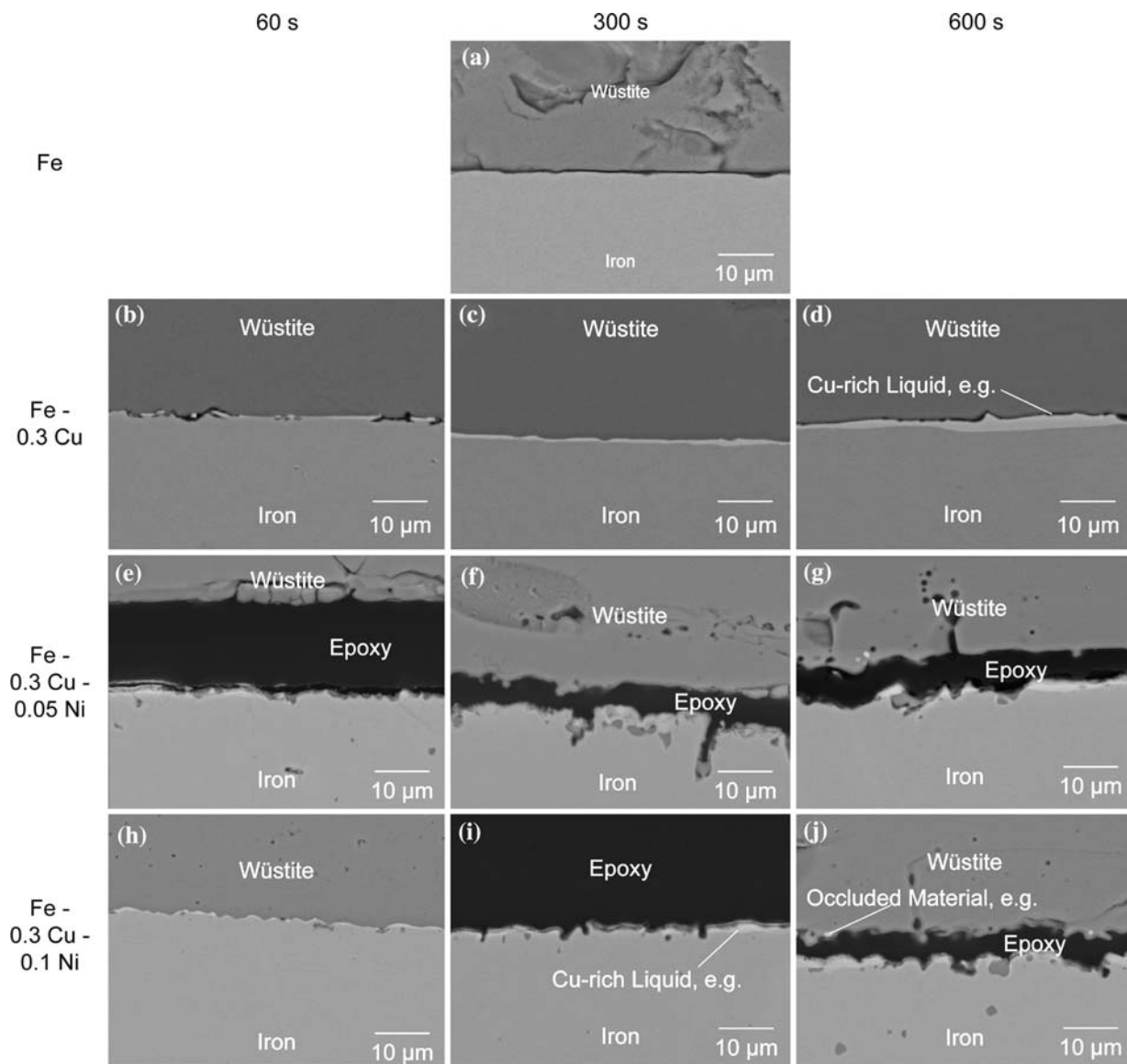


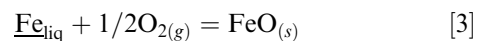
Fig. 6—Images of oxide/metal interface after oxidation for each chemistry and time. (a) The oxide/metal interface for sample Fe given as a reference. (b) through (d) The oxide/liquid/solid interface evolution with time for Fe-0.3Cu. (e) through (g) The oxide/liquid/solid interface evolution with time for Fe-0.3Cu-0.05Ni. (h) through (j) The oxide/liquid/solid interface evolution with time for Fe-0.3Cu-0.1Ni.

Table II. Energy-Dispersive Spectroscopy Measurements of Copper/Nickel Ratio Values near the Oxide/Metal Interface

t (s)	Fe-0.3Cu-0.1Ni Copper/Nickel Ratio	Fe-0.3Cu-0.05Ni Copper/Nickel Ratio
60	2.6	2.6
300	2.4	2.1
600	2.6	2.5

For iron oxidation, the parabolic rate is determined by the diffusion of iron cations through the wüstite layer.^[24] The driving force for cation transport is a vacancy gradient that is determined by the oxygen activity in local equilibrium at the wüstite/magnetite and wüstite/metal interfaces. When the copper-rich liquid forms and the local equilibrium prevails at

the liquid/wüstite interface, the local equilibrium condition



must change, because the liquid phase has an iron content that is much lower than the solid phase. The oxygen activity (relative to the standard state of 1 atm O_2 at 1150 °C) for the interfacial equilibrium is given by

$$p_{O_2} = \frac{1}{(a_{Fe})^2} \exp \frac{2\Delta G_{FeO}^0}{RT} \quad [4]$$

Thus, as the iron activity decreases, the equilibrium oxygen pressure at the metal/wüstite interface increases, the vacancy concentration gradient becomes shallower, and the oxidation rate should decrease. Although the liquid phase is copper rich, the iron-copper system

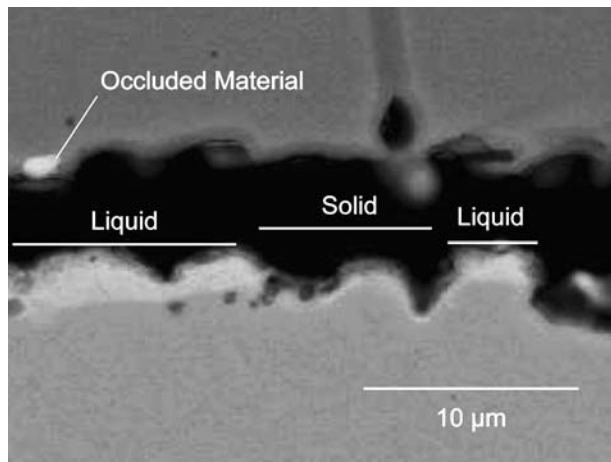


Fig. 7—Oxide/metal interface of sample Fe-0.3Cu-0.1Ni oxidized for 600 s. Indicated are the alternating regions of solid and liquid phase found at the oxide/metal interface as well as an example of material occluded into the oxide.

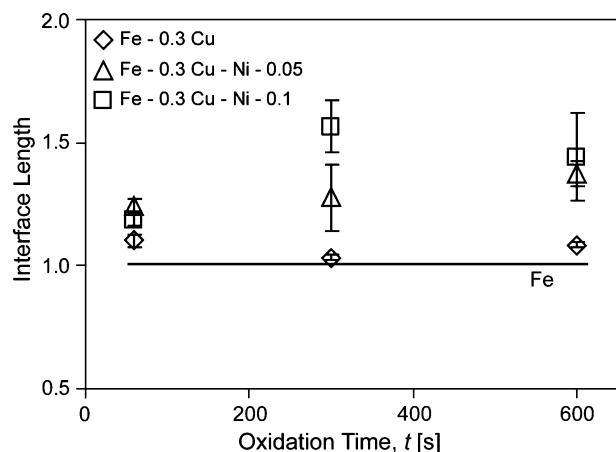


Fig. 8—Interface lengths (normalized to a flat interface) for samples investigated in this work. The line for pure iron is shown as a reference and is based off a 300 s oxidation experiment.

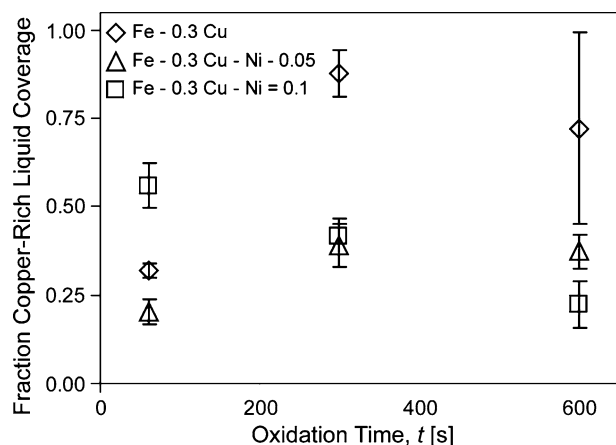


Fig. 9—Fraction of oxide/metal interface covered by copper-rich liquid.

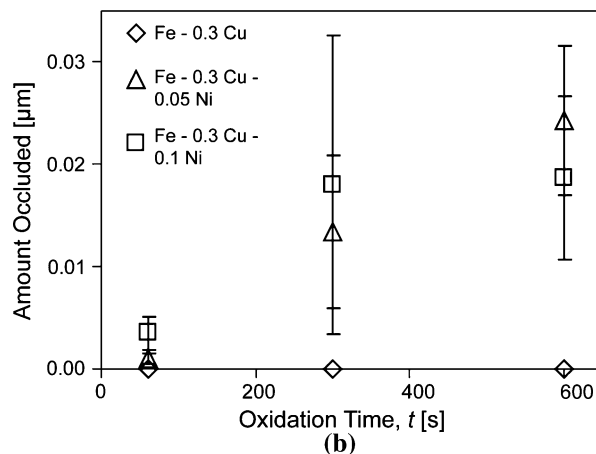
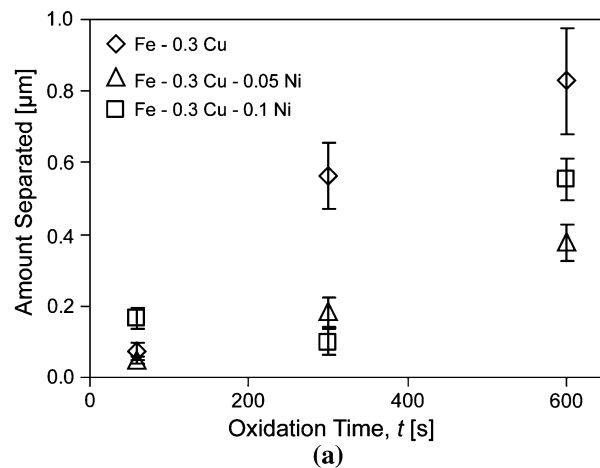


Fig. 10—Plots showing (a) amount of separated copper-rich liquid and (b) amount of occluded material.

exhibits positive deviations from ideality and, thus, the iron activity is higher than its mole fraction. Calculations using ThermoCalc,^{**[3]} with assessed data from

^{**}ThermoCalc is a trademark of Thermo-Calc Software, Stockholm, Sweden.

Chen and Jin^[4] show that the iron activity in the liquid phase is approximately 0.7 (pure fcc iron at 1150 °C as standard state and ignoring the presence of oxygen). Such a deviation from unit iron activity would not be expected to cause a significant change in the driving force for iron ion migration through the scale. Fast diffusion through the liquid phase maintains the iron concentration at this level; it is, therefore, reasonable to expect no effect on the oxidation rate when the liquid copper-rich phase is present. Interpreting the microstructure at the oxide/metal interface is straightforward. The oxidation of iron (and, therefore, the copper enrichment) should proceed at approximately the same rate over the entire sample, so a thin, uniform liquid layer is expected and observed. The schematic evolution of this microstructure is summarized in Figure 11(a).

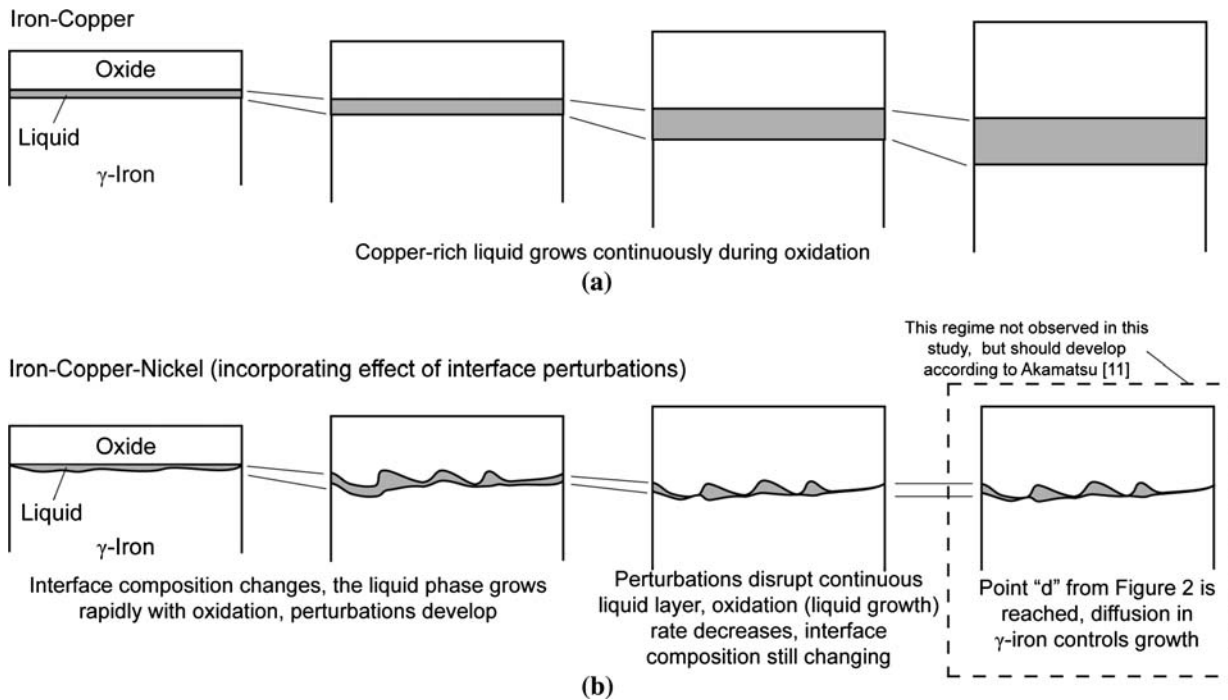


Fig. 11—Schematic evolution of interface microstructure for (a) iron-copper alloys and (b) iron-copper-nickel alloys incorporating effects of interface perturbations.

While copper alone does not affect the oxidation behavior, Figure 5(b) shows that copper + nickel additions do affect the parabolic oxidation rate of iron. A change in the oxide/metal interface microstructure (Figure 6) coincides with the decrease in oxidation rate. This interface morphology will be justified before the effect on oxidation behavior is discussed because the interface morphology influences the oxidation behavior. As shown in Figure 6, the microstructure at the oxide/metal interface consists of alternating regions of solid and liquid phases. The roughness of the oxide/metal interface is also increased, when copper and nickel are present (Figure 8). The effect of nickel on the interface roughness has been observed in several studies.^[11,14,25] Previous work on steels containing copper and nickel suggests that formation of the copper-rich liquid is delayed so that a rough oxide/metal interface develops.^[13,25] Subsequent occlusion of the enriched material prevents any further liquid-phase formation. These experiments all involved oxidation times longer than those investigated here and from the results shown here (Figure 6), it is apparent that a copper-rich liquid does form at relatively short times (at least 60 seconds). Because the presence of the liquid phase is expected to result in a planar oxide/metal interface,^[17] an explanation is necessary for the development of a rough interface in the presence of the copper-rich liquid.

It is first necessary to place the experimental results in the context of Figure 2 and the discussion presented in Section I of this work. The results suggest that the samples studied here are in the regime in which the interface composition is still adjusting along the phase boundary. If the interface composition had reached point d in Figure 2, the oxidation rate would be

controlled by iron diffusion in the γ -iron phase, rather than iron ion migration in the oxide. For binary iron-nickel alloys, oxidation rates decrease by two to three orders of magnitude compared to pure iron,^[26] when diffusion in the solid metal controls the overall oxidation rate. This is significantly larger than the decrease measured here. In addition, the EDS measurements of Table II suggest that some motion along the phase boundary has occurred, because the interface copper/nickel ratios are not equal to those in the bulk. Although the copper/nickel ratios measured by EDS in Table II show no evolution, EDS is not a sensitive enough analytical technique to be used as evidence against the reasoning used here. Thus, diffusion in the metal has likely not assumed the controlling role in the enrichment processes. The point at which diffusion in the γ -iron phase controls the overall oxidation rate was not observed in this study, nor was it experimentally observed by Akamatsu.^[11]

Although alloy diffusion does not control the evolution of the liquid phase, it still plays a role in the motion of the solid/liquid interface. It is proposed here that the rough interface develops due to processes at the liquid/solid-metal interface, not at the oxide/metal interface. The observed microstructure shown in Figure 6 is a result of both the interface microstructure evolution and the creep of the oxide to maintain contact with the interface. The development of a rough solid/liquid interface can be justified by examining the ternary diffusion phenomena occurring during oxidation. The problem is best formulated as a diffusion couple of copper-rich liquid with γ -iron. It is well known that wavy interfaces (essentially two-phase regions) can develop in diffusion couples of ternary alloys,^[27] because

concentration gradients are permissible across two-phase regions. Two-phase regions cannot develop in binary-alloy diffusion couples because there can be no concentration gradient across a two-phase region and, thus, no driving force for a growth (hence, the planar solid/liquid interface in the sample Fe-0.3 Cu).

Interface motion is a balance between the removal of the iron due to the oxidation and the diffusion of the copper and nickel back into the bulk metal. The discussion here focuses solely on the copper and nickel diffusion in γ -iron with oxidation acting independently to increase the thickness of the copper-rich layer and not playing a role in the interface microstructure development. The system can be viewed as a diffusion couple of copper-rich liquid and γ -iron with an initially planar liquid/ γ -iron interface. The planar interface breaks down in the presence of nickel, leading to the observed microstructure.

The analysis of interface stability has been treated by Mullins and Sekerka,^[28] for the solidification of binary alloys; by Wagner^[16] and Whittle *et al.*,^[29] for the oxidation of binary alloys; and by Coates and Kirkaldy, for ternary-alloy diffusion.^[30] The problem of interface stability in solid-state systems is most often discussed in the context of Wagner's calculations; there is a qualitative discussion in work done by Harrison and Wagner.^[31] This qualitative description predicts that a perturbation is stable if the concentration gradient responsible for the interface advancement is increased by the formation of a perturbation. While this qualitative understanding is intuitive, the condition is limited in that it assumes binary diffusion, in which the flux of any component depends only on its own concentration gradient.

In the ternary iron-copper-nickel alloy here, fluxes are represented by the following expressions:

$$j_{\text{Cu}} = \tilde{D}_{\text{CuCu}}^{\text{Fe}} \frac{\delta c_{\text{Cu}}}{\delta x} - \tilde{D}_{\text{CuNi}}^{\text{Fe}} \frac{\delta c_{\text{Ni}}}{\delta x} \quad [5]$$

$$j_{\text{Ni}} = \tilde{D}_{\text{NiNi}}^{\text{Fe}} \frac{\delta c_{\text{Ni}}}{\delta x} - \tilde{D}_{\text{NiCu}}^{\text{Fe}} \frac{\delta c_{\text{Cu}}}{\delta x} \quad [6]$$

$$j_{\text{Fe}} = j_{\text{Cu}} - j_{\text{Ni}} \quad [7]$$

In Eqs. [5] through [7], j represents the interdiffusion fluxes and D represents the interdiffusion coefficient. An

examination of Eqs. [5] through [7] shows that the copper and nickel flux is dependent on the concentration gradients of both species.

Studies by Clark and Rhines,^[32] Kirkaldy and Brown,^[33] and Wirtz and Dayananda^[34] (among others) have demonstrated that nonplanar interfaces form in ternary diffusion couples if measured diffusion paths enter two-phase regions at angles to tie lines. Kirkaldy and Brown^[33] have proposed using a virtual path (a calculated diffusion path^[33,35]) in a similar manner, to predict the formation of nonplanar interfaces. The entry of the virtual path into a two-phase region implies a supersaturation that is relieved by the precipitation of the second phase or the formation of interface perturbations. Coates and Kirkaldy have developed elementary^[36] and sophisticated^[30] mathematical expressions of criteria for interface stability.

Since rapid diffusion in the liquid would likely minimize any supersaturation, only the diffusion path in γ iron has been solved here. The path is generated by using solutions given by Kirkaldy and Young.^[35] The solution assumes the γ iron is semi-infinite, with a constant composition in the solid at the liquid/ γ -iron interface and a bulk-alloy composition infinitely far from the interface. As discussed earlier, with reference to Figure 2, the composition in the γ iron at the interface is expected to vary as oxidation progresses, in order to accommodate the enriched nickel. Since this analysis is intended only to elucidate the possibility of an interface breakdown, it is carried out under the assumption that the interface composition is constant. Two liquid/ γ -iron interfaces (Table III) were chosen to represent the composition at the solid/liquid interface. The first composition was chosen such that its copper-to-nickel ratio is 2.5, similar to that measured at the liquid/ γ interface (Table II). The second was chosen to simulate behavior at a lower copper-to-nickel ratio, since the measured values in Table II are higher than the actual interface ratio values.

The final quantities necessary for solving the diffusion path are the values for the four interdiffusion coefficients. These are usually represented as a 2×2 matrix:

$$\tilde{D} = \begin{bmatrix} \tilde{D}_{\text{CuCu}}^{\text{Fe}} & \tilde{D}_{\text{CuNi}}^{\text{Fe}} \\ \tilde{D}_{\text{NiCu}}^{\text{Fe}} & \tilde{D}_{\text{NiNi}}^{\text{Fe}} \end{bmatrix} \quad [8]$$

The superscript Fe in Eq. [8] refers to the choice of iron as the solvent metal. This must be noted because the

Table III. Relevant Quantities for Iron-Copper-Nickel Diffusion Path Calculation in γ -Iron

Concentration/Diffusion Coefficient	Comment	Source
$c_{\text{Cu}}^{\gamma/L} = 10$ (wt pct)	ratio of copper and nickel interface concentrations approximately equal to experimentally measured values, Cu/Ni = 2.5	EDS measurements in current work
$c_{\text{Ni}}^{\gamma/L} = 4$ (wt pct)		
$c_{\text{Cu}}^{\gamma/L} = 14$ (wt pct)	ratio of copper and nickel interface concentrations chosen to examine the effects of lower Cu/Ni ratio	—
$c_{\text{Ni}}^{\gamma/L} = 11$ (wt pct)		
$\tilde{D}_{\text{CuNi}}^{\text{Fe}} = 0$	off-diagonal coefficients set equal to zero	—
$\tilde{D}_{\text{NiCu}}^{\text{Fe}} = 0$		
$\tilde{D}_{\text{CuCu}}^{\text{Fe}} = 5.2 \times 10^{-10}$ (cm ² /s)	from averaged data in binary iron-copper alloy diffusion	Majima and Mitani ^[37]
$\tilde{D}_{\text{NiNi}}^{\text{Fe}} = 3.6 \times 10^{-11}$ (cm ² /s)	from averaged data in binary iron-nickel alloy diffusion	Hanatake <i>et al.</i> ^[38]

interdiffusion coefficients depend on the choice of solvent.^[35]

Diffusion coefficient data for the ternary iron-copper-nickel system at 1150 °C do not exist. Rönkä *et al.*^[39] have evaluated interdiffusion coefficients in the iron-copper-nickel system at 1000 °C and found that the off-diagonal elements $\tilde{D}_{\text{CuNi}}^{\text{Fe}}$ and $\tilde{D}_{\text{NiCu}}^{\text{Fe}}$ (Eq. [8]) are nonzero and that there is significant concentration dependence to all of the diffusion coefficients. Attempts were made to include this concentration dependence by modeling with the software DICTRA.^{†[40]} However, this led to results

[†]DICTRA is a trademark of Thermo-Calc Software, Stockholm, Sweden.

that did not agree well with either the ternary data from Rönkä *et al.*^[39] at 1000 °C or the binary-alloy diffusivity data at 1150 °C presented in Table III. Therefore, a simplified representation, listed in Table III, was used in this study.

The results of the calculation discussed here are shown in Figure 12. Based on the simplified diffusivity matrix (Table III), the diffusion path in Figure 12(a)

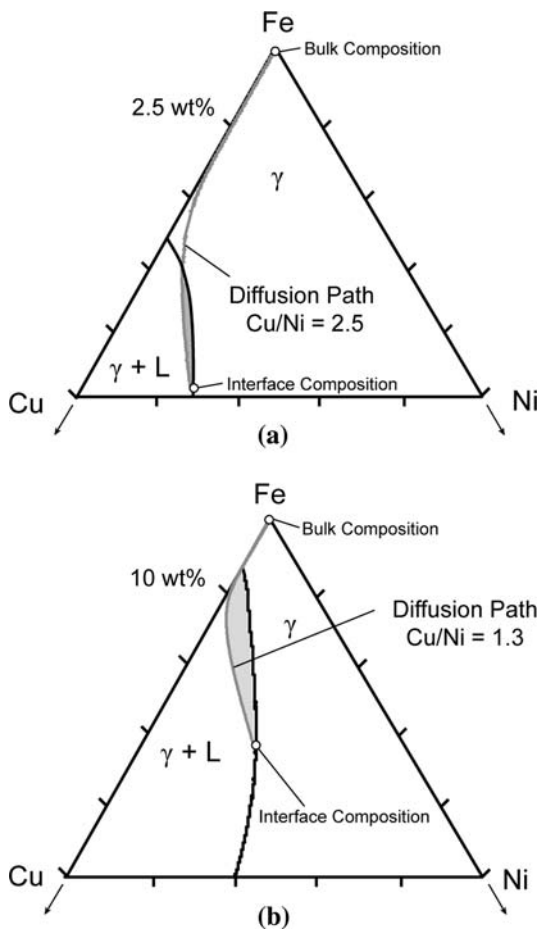


Fig. 12—Copper/nickel diffusion path plotted on the ternary isotherm for (a) Cu/Ni ratio measured from experimental results and (b) a lower Cu/Ni ratio than in (a). The gray line represents the diffusion path. The supersaturated region is shaded.

does enter the two-phase region (gray colored region). The unphysical nature of this solution indicates that a planar solid/liquid interface could indeed be unstable under the present experimental conditions. If the EDS measurements are indeed too high, decreasing the copper/nickel ratio at the liquid/ γ -iron interface drives the path further into the two-phase region; a planar interface, therefore, is still unstable.

A criterion for interface breakdown has also been discussed by Wirtz and Dayananda,^[34] it is based on the expression for the interfacial mass balance between two phases. These authors suggest that interface breakdown occurs because interface compositions defined by a single tie line on the phase diagram (*i.e.*, a planar interface) cannot satisfy the interfacial mass balance criteria for all components. This occurs because the interdiffusion fluxes near the interface for different components are generally unequal. This is the case for the present system, as implied by the curved diffusion path in Figure 12. In addition, the differences in the interface composition between the liquid and solid phases (Figure 2, $c_{\text{Cu}}^{\gamma/L} > c_{\text{Cu}}^{L/\gamma}$ and $c_{\text{Ni}}^{\gamma/L} < c_{\text{Ni}}^{L/\gamma}$) predict that the interface velocity will be of a different sign, depending on whether copper or nickel is used for the calculation. Thus, the criterion of Wirtz and Dayananda^[34] also suggests that the development of the microstructure near the oxide/metal interface shown in Figure 6 is very likely due to the breakdown of a planar liquid/ γ -iron interface.

In order to investigate the sensitivity to the off-diagonal terms in the diffusivity matrix (which were assumed zero for the calculation), calculations were repeated with values assigned to the off-diagonal diffusion coefficients. Since there are no data at the experimental temperature for this system, numbers of the same order of magnitude as the on-diagonal diffusivities were chosen for the investigation. While the off-diagonal diffusion coefficients were found to affect the shape of the path, no combination was found that would prevent the path from entering the two-phase region.

From these results and the earlier discussion, it is likely that a planar solid/liquid interface should not be stable in the iron-copper-nickel system. As the interface microstructure evolves, the continuous liquid layer could be disrupted, leaving alternating regions of solid and liquid and causing the interface length increase observed in Figure 8. This type of morphology is observed experimentally, as shown in Figures 6(e) through (j) and Figure 7, and is indicated schematically in Figure 11(b). This analysis represents a different approach to the formation of a perturbed oxide/metal interface. Current understanding suggests that the appearance of a copper-rich liquid phase is generally assumed to lead to a planar interface^[15,17] and that nickel delays the formation of the liquid layer until perturbations in the oxide/metal interface stabilize.^[13,15] However, Figure 6(h) clearly shows a perturbed interface in the presence of a liquid layer. Thus, the theory developed in this work appears to be a better justification for the oxide/metal interface microstructure.

This observed breakdown of the liquid layer into isolated pockets is a likely cause for the observed

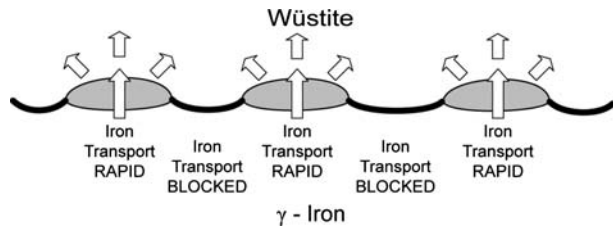


Fig. 13—Schematic showing the iron supply paths during oxidation of iron-copper-nickel alloys with the simplifying assumption that transport through the solid regions is negligible.

decrease in the oxidation rate. As shown in Figure 5(b), the parabolic rate of the nickel-containing samples decreases by approximately a factor of 2 from pure iron or Fe-0.3 Cu. For oxidation to proceed, iron must be supplied to the oxide/metal interface through the alternating liquid and solid phases. Given that the iron diffusion in the solid alloy is extremely slow compared to the diffusion in wüstite or in the copper-rich liquid, the iron supply to the oxide from these solid regions would be effectively negligible. Thus, all of the iron comes from transport through the liquid regions. A schematic of this is shown in Figure 13.

Figure 13 shows that the two-phase interface microstructure effectively limits the area over which iron is supplied to the wüstite. Overall, however, the wüstite appears as a layer of uniform thickness, because rapid lateral diffusion supplies iron ions to the regions of wüstite that are above the solid alloy. A new rate constant accounting for this decrease in area can be calculated, if both the rate constant of a liquid-covered interface and the fraction coverage are known. Both of these values have been measured. Since the effects are only in the parabolic regime of oxidation, the rate expression is

$$\left(\frac{\Delta m}{A_{\text{liquid}}}\right) = \sqrt{k_p^{\text{liquid}} t} \quad [9]$$

In the Fe-0.3Cu-0.05Ni and Fe-0.3Cu-0.1Ni samples, $A_{\text{liquid}} = fA_{\text{sample}}$, where f is the liquid-phase fraction covering the surface (~0.4, according to Figure 9); Eq. [9] then becomes

$$\frac{1}{f} \left(\frac{\Delta m}{A_{\text{liquid}}}\right) = \sqrt{k_p^{\text{liquid}} t} \quad [10]$$

The quantity $(\Delta m/A_{\text{sample}})$ is the mass gain over the total sample area (data measured in Figure 4). Thus,

$$\frac{1}{f} \sqrt{k_p^{\text{total}} t} = \sqrt{k_p^{\text{liquid}} t} \quad [11]$$

After rearranging terms and canceling time,

$$k_p^{\text{total}} = f^2 k_p^{\text{liquid}} \quad [12]$$

Since $k_p^{\text{liquid}} = k_p^{\text{pure iron}} = 6 \text{ mg}^2/\text{cm}^4 \text{ s}$, and $f = 0.4$, the calculated k_p^{total} from Eq. [12] is $1 \text{ mg}^2/\text{cm}^4 \text{ s}$. This value is of the same order of magnitude as the measured

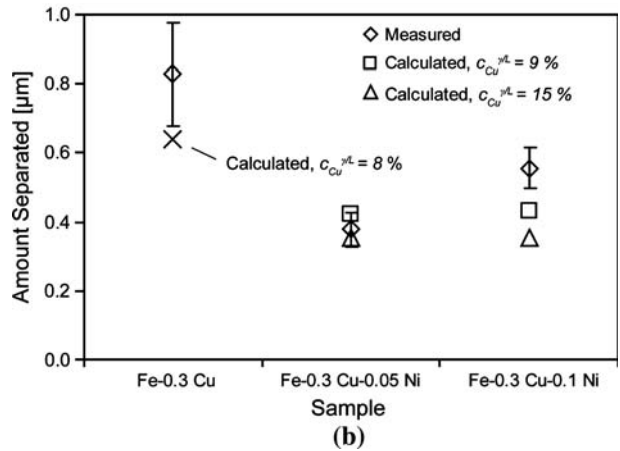
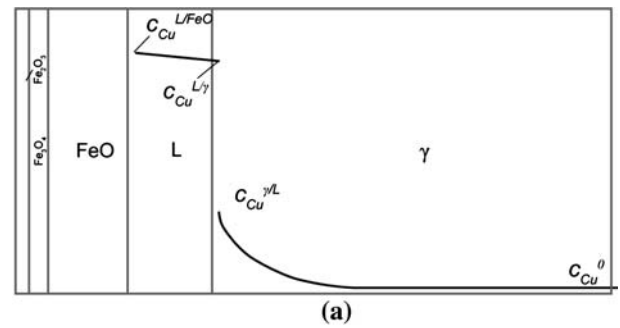


Fig. 14—(a) Schematic of phase arrangements and concentration gradients for numeric model.^[41] (b) Comparison between measured and calculated amount of copper-rich liquid formed after 600 s oxidation for the different sample chemistries studied in this work.

rate constant, $2.5 \text{ mg}^2/\text{cm}^4 \text{ s}$. The difference between the two values suggests that the iron supply from the solid phase may not be completely blocked, as assumed. It should be noted that this theory will require more justification with samples oxidized for longer times and varying nickel contents before it can be considered completely valid. In addition, as mentioned here, the estimate for the parameter f was conservative. The enlarged image of the interface region shown in Figure 7 shows that some areas of the region labeled solid may, indeed, be liquid. It is not readily apparent, however, whether these brighter areas are very thin liquid films or are the rounding of the edges of the metal due to polishing. Thus, the calculation was performed with the conservative estimate of the copper-rich coverage.

Nickel additions decrease the amount of separated copper-rich liquid and increase the amount of occluded material (Figure 10), compared to sample Fe-0.3 Cu. The decrease in the amount of separated copper can be attributed to one of two factors: either the decrease in oxidation rate or the increase in amount occluded. Since the measured amount of occluded material is much less than the measured amount of separated material, it is likely that the decreased oxidation rate was the primary cause of the reduction in the copper-rich liquid.

The effects of a decrease in the oxidation rate can be approximated with a numeric model developed by the present authors.^[41] This model predicts the evolution of the copper-rich liquid for a given oxidation kinetics by

Table IV. Values Used to Approximate Effects of Nickel in a Copper Enrichment Model Developed by the Authors

Sample	$c_{\text{Cu}}^{\gamma/L}$ (Wt Pct)
Fe-Cu, Figure 1	8
Fe-Cu-Ni, for Cu/Ni = 2.5	9
Fe-Cu-Ni, for Cu/Ni = 1.3	15

examining the mass balance of copper. A schematic of the problem setup for the model is shown in Figure 14(a). It is important to note that the model does not account either for the effects of the ternary diffusion discussed here or for nonplanar interfaces. It also does not account for the evolution in the interface composition shown schematically in Figure 2. Although diffusion of copper and nickel into the steel is important for determining the interface microstructure, it alone does not significantly affect the amount of copper-rich liquid formed during oxidation. Therefore, the model can still be used to estimate the effect of the decrease in the oxidation rate.

The effect of the evolution of the interface composition is approximated by choosing values of $c_{\text{Cu}}^{\gamma/L}$, the solubility of copper in iron, that correspond to the point measured by EDS (Table II). As indicated earlier, a value corresponding to a copper/nickel ratio of 1.3 was chosen, to determine whether an overestimate by EDS affects the results. The values used for this parameter are shown in Table IV. Comparisons between the amounts of separated copper-rich liquid are shown in Figure 14(b).

Although the model considers the copper-rich liquid only as a thin layer at the interface, and not the alternating solid/liquid regions, as observed, it adequately predicts the final amount of separated copper regardless of the value for $c_{\text{Cu}}^{\gamma/L}$. This result suggests that the decrease in the amount of separated material can be attributed to the decrease in the oxidation rate, rather than to an increase in occlusion. These results support the previous conclusion that the presence of silicon is necessary for occlusion, under the conditions studied. Significant occlusion can be observed in steels without silicon, but only after longer oxidation times,^[14,42] higher oxidation temperatures,^[25] or changes in the oxidizing atmosphere.^[15]

This work expands the original enrichment description proposed by Akamatsu *et al.*,^[11] by incorporating the effects of a nonplanar solid/liquid interface. The major effect of this interface microstructure is to decrease the oxidation rate and, therefore, the liquid growth rate at an earlier time than would be expected by assuming the copper-rich liquid was present as a uniformly distributed layer (Figure 11).

V. CONCLUSIONS

From this study, the following conclusions were drawn.

1. With small amounts of added copper, a thin, copper-rich liquid layer forms at the oxide/metal interface.

- Because of the fast transport through this liquid layer and positive deviations from ideality in the iron-copper system, the iron oxidation rate is unaffected.
- Nickel + copper additions decrease the oxidation rate by a factor of 2. The interface microstructure consists of alternating solid/liquid regions.
 - The interface microstructure is a consequence of the breakdown of the planar solid/liquid interface from the unequal copper and nickel diffusivities in the solid metal. This was justified by the examination of a diffusion path calculation in the γ -iron phase.
 - The decrease in the oxidation rate was justified by assuming that iron can be transported to the oxide only through the liquid regions (transport through the solid is too slow).
 - Nickel additions decrease the amount of separated copper-rich liquid, compared to an iron-copper alloy. A comparison with the predictions of a model that simulates copper-rich liquid evolution shows that the decrease in the oxidation rate accounts for the decrease in the amount separated.
 - Nickel additions alone do not lead to substantial occlusion during short-time oxidation.

ACKNOWLEDGMENTS

The authors gratefully acknowledge the financial support from the Center for Iron and Steelmaking Research, Carnegie Mellon University (Pittsburgh, PA), and the Pennsylvania Infrastructure Technology Alliance.

REFERENCES

- J.A.T. Jones, B. Bowman, and P.A. Lefrank: *The Making, Shaping, and Treating of Steel—Steelmaking and Refining Volume*, 11th ed., The AISE Steel Foundation, Pittsburgh, PA, 1998, pp. 525–660.
- Energetics Inc.: *Energy and Environmental Profile of the U.S. Iron and Steel Industry*, DOE/EE-0229, United States Department of Energy, Office of Industrial Technologies, Washington, DC, 2000, pp. 10–26.
- B. Sundman, B. Jansson, and J.-O. Andersson: *CALPHAD: Computer Coupling of Phase Diagrams and Thermochemistry*, 1985, vol. 9, pp. 153–90.
- Q. Chen and Z. Jin: *Metall. Mater. Trans. A*, 1995, vol. 26A, pp. 417–26.
- S. Pötschke and A.R. Büchner: *Steel Res. Int.*, 2006, vol. 77, pp. 416–22.
- A. Nicholson and J.D. Murray: *J. Iron Steel Inst.*, 1965, vol. 203, pp. 1007–18.
- D.A. Melford: *J. Iron Steel Inst.*, 1962, vol. 200, pp. 290–99.
- W.J.M. Salter: *J. Iron Steel Inst.*, 1966, vol. 204, pp. 478–88.
- Handbook of Ternary Alloy Phase Diagrams*, P. Villars, A. Prince, and H. Okamoto, eds., ASM INTERNATIONAL, Metals Park, OH, 1995, pp. 9350–91.
- B. Yalamanchili, P. Power, and J. Nelson: *Wire J. Int.*, 1999, vol. 32, pp. 143–55.
- S. Akamatsu, T. Senuma, Y. Takada, and M. Hasebe: *Mater. Sci. Technol.*, 1999, vol. 15, pp. 1301–07.
- S.V. Divinski, F. Hisker, C. Herzig, R. Filipek, and M. Danielewski: *Def. Diff. Forum*, 2005, vols. 237–240, pp. 50–61.
- G.L. Fisher: *J. Iron Steel Inst.*, 1969, vol. 207, pp. 1010–16.
- T. Fukagawa and H. Fujikawa: *Oxid. Met.*, 1999, vol. 52, pp. 177–94.
- R.Y. Chen and W.Y.D. Yuen: *ISIJ Int.*, 2005, vol. 45, pp. 807–16.

16. C. Wagner: *J. Electrochem. Soc.*, 1956, vol. 103, pp. 571–80.
17. H.J. Grabke, V. Leroy, and H. Viehhaus: *ISIJ Int.*, 1995, vol. 35, pp. 95–113.
18. B.A. Webler and S. Sridhar: *ISIJ Int.*, 2007, vol. 47, pp. 1245–54.
19. H. Abuluwefa, R.I.L. Guthrie, and F. Ajersch: *Oxid. Met.*, 1996, vol. 46, pp. 423–40.
20. W. Rasband: ImageJ, Windows version 1.36, US National Institutes of Health, Bethesda, MD.
21. R.Y. Chen and W.Y.D. Yuen: *Oxid. Met.*, 2003, vol. 59, pp. 433–68.
22. K. Schwerdtfeger and S. Zhou: *Steel Res.*, 2003, vol. 74, pp. 538–48.
23. V.G. Levich: *Physicochemical Hydrodynamics*, 1st ed., Prentice-Hall, Inc., Englewood Cliffs, NJ, 1962, p. 87.
24. L. Himmel, R.F. Mehl, and C.E. Birchenall: *Trans. AIME*, 1953, vol. 197, pp. 827–43.
25. R.Y. Chen and W.Y.D. Yuen: *Oxid. Met.*, 2005, vol. 63, pp. 145–68.
26. R.T. Foley: *J. Electrochem. Soc.*, 1962, vol. 109, pp. 1202–06.
27. F.J.J. Van Loo: *Prog. Solid State Chem.*, 1990, vol. 20, pp. 47–99.
28. W.W. Mullins and R.F. Sekerka: *J. Appl. Phys.*, 1964, vol. 35, pp. 444–51.
29. D.P. Whittle, D.J. Young, and W.W. Smeltzer: *J. Electrochem. Soc.*, 1976, vol. 123, pp. 1073–79.
30. D.E. Coates and J.S. Kirkaldy: *Trans. ASM*, 1969, vol. 62, pp. 426–36.
31. J.D. Harrison and C. Wagner: *Acta Metall.*, 1959, vol. 7, pp. 722–35.
32. J.B. Clark and F.N. Rhines: *Trans. ASM*, 1959, vol. 51, pp. 199–221.
33. J.S. Kirkaldy and L.C. Brown: *Can. Metall. Q.*, 1963, vol. 2, pp. 89–117.
34. L.E. Wirtz and M.A. Dayananda: *Metall. Trans. A*, 1977, vol. 8A, pp. 567–75.
35. J.S. Kirkaldy and D.Y. Young: *Diffusion in the Condensed State*, 1st ed., The Institute of Metals, London, 1987, pp. 163 and 361–400.
36. D.E. Coates and J.S. Kirkaldy: *J. Cryst. Growth*, 1968, vols. 3–4, pp. 549–54.
37. K. Majima and H. Mitani: *Trans. Jpn. Inst. Met.*, 1978, vol. 19, pp. 663–68.
38. Y. Hanatate, K. Majima, and H. Mitani: *Trans. Jpn. Inst. Met.*, 1978, vol. 19, pp. 669–73.
39. K.J. Rönkä, A.A. Kodentsov, P.J.J. Van Loon, J.K. Kivilahti, and F.J.J. Van Loo: *Metall. Mater. Trans. A*, 1996, vol. 27A, pp. 2229–38.
40. A. Borgenstam, L. Höglund, J. Ågren, and A. Engström: *J. Phase Equilib. Diffus.*, 2000, vol. 21, pp. 269–80.
41. B.A. Webler and S. Sridhar: *Def. Diff. Forum*, 2008, vols. 273–276, pp. 713–23.
42. N. Imai, N. Komatsubara, and K. Kunishige: *ISIJ Int.*, 1997, vol. 37, pp. 224–31.